THE JOURNAL OF PHYSICAL CHEMISTRY C
A JOURNAL OF THE AMERICAN CHEMICAL SOCIETY

pubs.acs.org/JPCC

Article

Role of La 5p in Bulk and Quantum-Confined Solids Probed by the La $5p^5 4f^1$ $^3D_1$ Excitonic Final State of Resonant Inelastic X-ray Scattering

Chun-Yu Liu,* Ping Feng, Kari Ruotsalainen, Karl Bauer, Régis Decker, Maximilian Kusch, Katarzyna E. Siewierska, Annette Pietzsch, Markus Haase, Yan Lu, Frank M. F. de Groot, and Alexander Föhlisch*

Cite This: J. Phys. Chem. C 2023, 127, 11111−11118

Read Online

ABSTRACT: The varied electronic localization of rare earth elements is essential to functional materials and a key to tailoring their properties. We establish with unprecedented spectral resolution the excitonic nature of the lanthanum $5p^5 4f^1$ $^3D_1$ and $^3D_2$ final states of resonant inelastic X-ray scattering (RIXS) at the La $N_{4,5}$ edges. We extract the intrinsic lifetime, energy distance, and relative intensity ratio from single crystal $LaAlO_3$ and construct an empirical model. With help of the model, we precisely determine the RIXS $^3D_1$ final state position and identify La 5p as a descriptor of covalency with the host material. For metallic lanthanum, La^{3+} ions in mixed-covalent-ionic simple oxides and phosphates, and ionic salts alike, we find a sizable chemical shift, indicating band-like and free-ion-like La. The different electronic relaxation of the La $5p^5$ hole and the La $4f^1$ electron is discussed with local and nonlocal screening contributions. In addition, the energetics of the excitonic La $5p^5 4f^1$ Coulomb attraction is quantified in its variation from lanthanum metal to mixed-covalent-ionic La_2O_3 and the ionic LaF_3 salt. The power of the approach and analysis is applied to map the influence of geometric quantum confinement to La 5p sharing within quantum dots and quantum wires in comparison to bulk-like microrods of monoclinic $LaPO_4$.

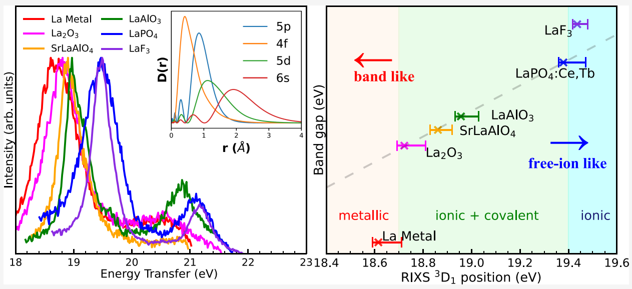

INTRODUCTION

The f-block rare-earth (RE) elements (La−Lu) are present in many compounds with a wide range of applications, including phosphors,[1−3] scintillators,[4,5] superconductors,[6,7] and solid-state lasers[8,9] as well as catalysts.[10−13] The RE elements are generally considered to be atomically localized species, mainly caused by their highly localized frontier orbitals.[14−19] This is in strong contrast to actinides, where the 5f orbital is spatially more diffused and evidenced to be involved in covalent bond formation.[20−23] However, recently both theoretical and experimental work suggested that the REs contribute to band formation and screening.[24−27] Do the 4f-block REs participate in chemical bonding, and which orbitals contribute to covalency? How can this be linked to material functionality? These still remain open questions.[28]

Lanthanum, the simplest RE element from an electronic structure perspective, occurs both as a metallic elemental solid with the electron configuration $[Xe]5d^1 6s^2$ and as the La^{3+} ion isoelectronic to Xe. The frontier atomic orbitals are composed of 5p, 6s, 4f, and 5d. It is known and established experimentally and theoretically from the RE series that in general the 4f states are barely perturbed by the host material, causing narrow 4f bands[29−32] and being considered "chemically inert". In the case of La, the unoccupied 4f shell lies even higher in energy scale and 4f orbital mixing with the ligand states is energetically highly unfavorable.[32,33] Even though some work suggested the contribution of RE 4f to chemical bond,[34−36] it appears mostly in higher oxidation states instead of typical trivalent compounds or in specific systems such as heavy fermions.[37,38] 5d and 6s shells' participation in chemical bonding, on the other hand, is generally accepted.[34,39,40] The contribution to covalency from pseudocore (inner valence) 5p shell is still unclear.[41,42] In lanthanides, the 5p shell is spatially extended and penetrates into the core (Figure 1) which effectively screens the 4f shell;[43] hence it is more favorable than the 4f shell to form a spatial-driven covalent bond. Previous experimental and theoretical studies indicate that the 5p in the electronic structure yields a ≈20 eV shallow potential that makes covalent bonding possible through inner valence

Received: March 27, 2023
Revised: May 12, 2023
Published: June 1, 2023

https://doi.org/10.1021/acs.jpcc.3c02011
J. Phys. Chem. C 2023, 127, 11111−11118

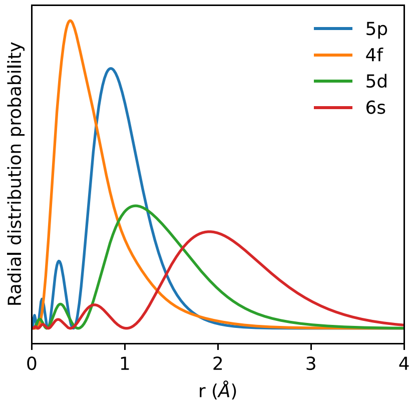

Figure 1. Illustrative radial distribution probability for 5p, 4f, 5d, and 6s atomic orbitals of La^{3+}. The wave functions are calculated at Hartree–Fock level with segmented all-electron relativistically contracted basis sets and ZORA relativistic Hamiltonian from Orca package.[46] The wave functions are analyzed by Multiwfn program.[47]

molecular orbital formation.[35,44,45] Note that throughout this article, we define the intraactomic orbital hybridization (e.g., sp^3 of carbon in CH_4) as "hybridization", and interatomic metal–ligand bond as "orbital mixing".

With resonant inelastic X-ray scattering (RIXS) we can gain insights into the energy and dynamics of charge, lattice, spin, and collective excitations in solids and molecules.[48,49] The RIXS energy loss or energy transfer quantifies the excitation energy transferred to intrinsic excitations of the scatterer and its host material. Lanthanum maintains in both its neutral metallic charge state and La^{3+} ionic state an empty $4f^0$ shell. Thus, RIXS at the La $N_{4,5}$ edges leads always to a well-defined La $5p^5 4f^1$ final state independent of the host material.

In this work, we establish with unprecedented spectral resolution the excitonic nature of the lanthanum $5p^5 4f^1$ $^3D_1$ final state in RIXS at the La $N_{4,5}$ edges and identify La 5p as a descriptor of covalency. This is driven by both ground-state interaction and the final state screening. For a systematic evaluation of the various host materials, we compare metallic lanthanum with a series of La^{3+} simple oxides, phosphates, and fluoride. We observe scaling of the La $5p^5 4f^1$ final state energy in mixed-covalent-ionic solid La^{3+} systems with an increasing band gap. The term "mixed-covalent-ionic" denotes ionic crystals having a partially covalent character due to polarized valence electrons. Metallic La is screened to a deviating, overall lower La $5p^5 4f^1$ final state energy. Ionic LaF_3 with highly electronegative fluoride is at a deviating, overall higher La $5p^5 4f^1$ final state energy. The different electronic relaxation of the La $5p^5$ hole and the La $4f^1$ electron is discussed with local and nonlocal screening contributions. In addition, the energetics of the excitonic La $5p^5 4f^1$ Coulomb attraction is quantified from underlying apparent screening factors. The power of the approach and analysis is applied to follow the influence of geometric quantum confinement to La 5p sharing within shape-engineered quantum dots and quantum wires in

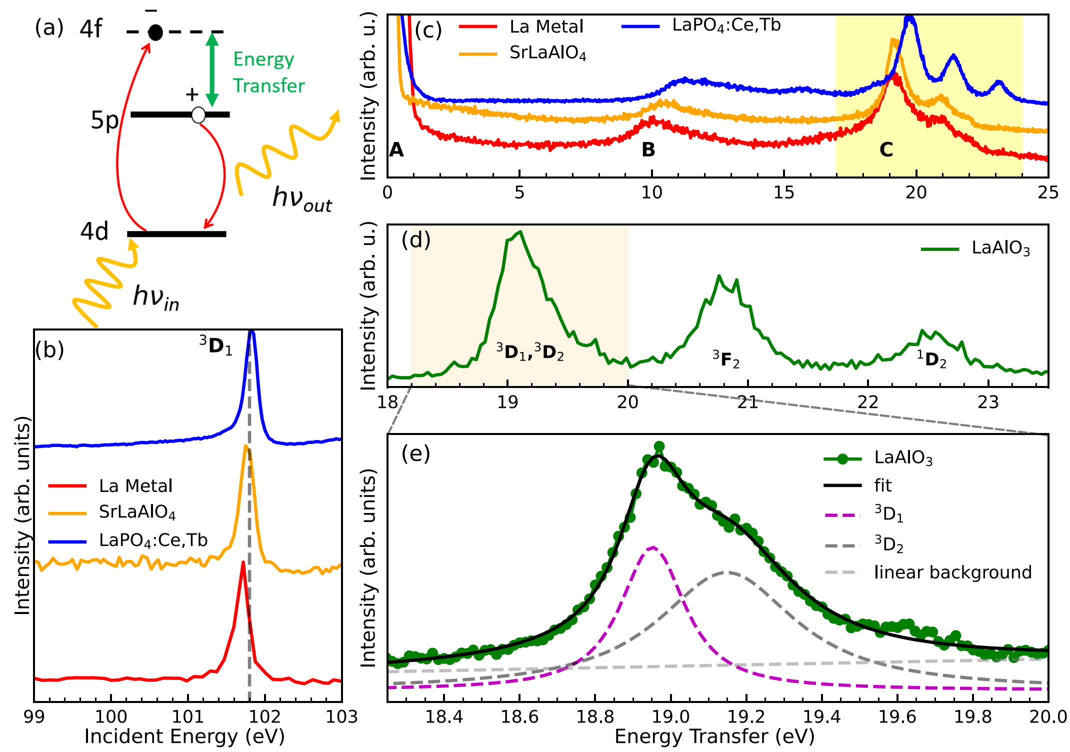

Figure 2. (a) Scheme of resonant inelastic X-ray scattering (RIXS) leading independently of the lanthanum chemical state (metallic La or La^{3+}-ion) via the $4d^9 4f^1$ $^3D_1$ core-excited state to the excitonic La $5p^5 4f^1$ $^3D_1$ final state. The excitonic nature of La $5p^5 4f^1$ $^3D_1$ gives a signature to quantify La 5p covalent sharing. (b) X-ray absorption (XAS) step of the RIXS process created by resonantly core-excited $4d^9 4f^1$ $^3D_1$ multiplet state (La metal and $LaPO_4$:Ce,Tb in total electron yield; $SrLaAlO_4$ in fluorescence yield). (c) RIXS via the La $4d^9 4f^1$ $^3D_1$ core-excited state. Region A: participator or resonant elastic channel. Region B: charge transfer and charge fluctuation channel. Region C: La $5p^5 4f^1$ final state with four multiplet states, as shown in panel. (d) La $5p^5 4f^1$ final state with four multiplet states ($^3D_1$, $^3D_2$, $^3F_2$, and $^1D_2$). (e) High-resolution RIXS spectrum and peak assignment of the $^3D_1$ and $^3D_2$ terms. All further analyses are based on the $^3D_1$ energy transfer peak position.

https://doi.org/10.1021/acs.jpcc.3c02011
J. Phys. Chem. C 2023, 127, 11111−11118

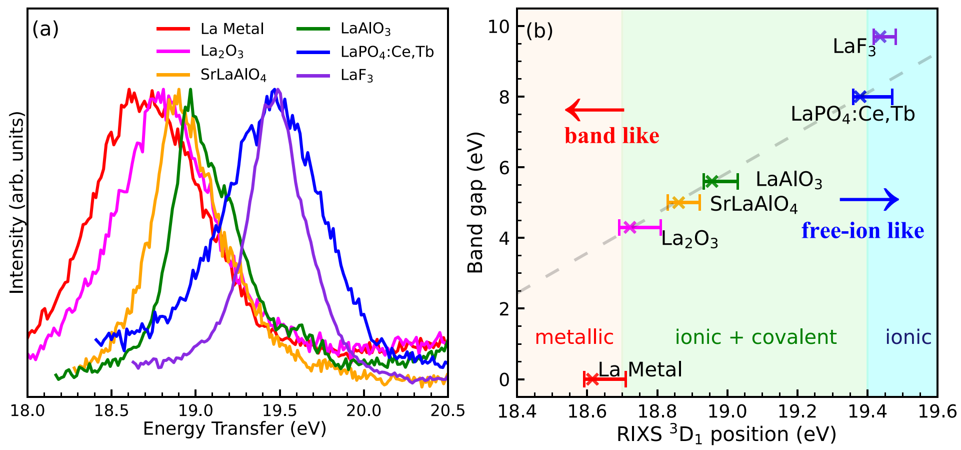

Figure 3. (a) High-resolution RIXS spectra of the La $5p^5 4f^1$ $^3D_1$ and $^3D_2$ final states of lanthanum metal, La_2O_3, $SrLaAlO_4$, $LaAlO_3$, $LaPO_4$:Ce,Tb, and LaF_3. (b) La $5p^5 4f^1$ $^3D_1$ peak position derived from the spectra of Figure 3a vs band gaps reported in the literature. The values are summarized in Table 1. The linear regression is restricted to the mixed-covalent-ionic system and has R^2 = 0.999.

comparison to bulk-like microrods of mixed-covalent-ionic $LaPO_4$.

EXPERIMENTAL SECTION

The X-ray absorption spectroscopy (XAS) and RIXS experiments were performed at BESSY-II (Helmholtz-Zentrum Berlin) at beamline U49[50] with the SolidFlexRIXS end station[51] for the overview RIXS spectra and at the UE112-PGM1 with the meV-RIXS permanent end station[52] for the high-resolution RIXS spectra. The measurements were carried out at room temperature at 10^{-8} mbar pressure with a linearly polarized beam. The supporting XAS spectra were collected with total electron yield (TEY) or fluorescence yield at 0.05 or 0.1 eV step. The excitation energy for RIXS was chosen at the XAS $^3D_1$ pre-edge resonance maximum position (101.8 ± 0.1 eV). The high-resolution RIXS spectra were acquired from the meV-RIXS spectrometer and were composed of fwhm ≈ 45–60 meV instrumental resolution and samples' natural lifetime and chemical broadening. Eight different La-containing samples were investigated in this work and were sorted as follows. Samples from noncommercial sources were obtained from the referenced source. Single crystal: $LaAlO_3$ (Alineason), $SrLaAlO_4$ (Alineason). Polycrystalline: La metal (99.9%, Alfa Aesar), LaF_3 (broken crystal, Alfa Aesar). Amorphous powder: La_2O_3 (99.9%, Alfa Aesar). Nanoparticles: $LaPO_4$:Ce,Tb quantum dot (QD),[2] $LaPO_4$ 30 nm quantum wire (QW, synthesis modified from Riwotzki et al.[53]), and $LaPO_4$ microrod (synthesis modified from Wang et al).[54] Characterization and detailed synthesis are provided in Supporting Information Figures S4–S6.

RESULTS AND DISCUSSION

Figure 2a depicts how the La $5p^5 4f^1$ final state is created in RIXS at the La $N_{4,5}$ edges. In the first step, XAS at the La $N_{4,5}$ edges, the La 4d electron is excited to the La $4d^9 4f^1$ core-excited intermediate state. Then, radiative decay leads to La $5p^5 4f^1$ final state, which occurs for lanthanum independent of it being neutral or ionic. In detail, the XAS step in lanthanum is characterized by a dipole-allowed giant resonance and spin-forbidden satellite states, on which we focus in the present study. The dipole-allowed giant resonance is the strong symmetry-allowed transition from the 4d shell to the 4f state with $^1P_1$ symmetry. Since the contracted 4f radial wave function interacts significantly with the transiently created 4d core hole, Coulomb and exchange interactions lead to satellite multiplets below the giant resonance. These spin-forbidden $^3P_1$, $^3D_1$ XAS satellites of lanthanum are reached via spin–orbit coupling within the total angular momentum J = 1 manifold.[42,55−58] The atomic nature of the $^3P_1$ and $^3D_1$ states causes their presence for all lanthanum-containing systems alike independent of being neutral La or ionic La^{3+} or its specific chemical environment[42,57,59,60] (see Supporting Information, Figure S1). Charge-transfer satellites were not observed in all samples' XAS, which further indicates the chemically inert 4f states without intraatomic hybridization or orbital mixing with the ligands. The $^3D_1$ state has an order of magnitude higher absorption cross section in comparison to the $^3P_1$ state. We thus resonantly core excite our La containing systems always into the La $4d^9 4f^1$ $^3D_1$ absorption resonance as shown in Figure 2b at 101.8 eV (dashed lines in Figure 2b) with ±0.1 eV incident photon energy bandwidth and uncertainty. The slight system-dependent shifts on the sub (±0.1 eV) scale can be attributed to channel interference from the tailing of the $^1P_1$ giant resonance due to autoionization.[57] As shown in Figure 2c, this resonant excitation at the La $4d^9 4f^1$ $^3D_1$ absorption resonance leads to characteristic La RIXS spectra. Peak A is the participator or elastic contribution. Feature B is assigned to the charge transfer from the occupied ligand band to the empty 4f band ($4f^1\underline{L}$).[42] The intensity of peak B arises from the coupling of the $4f^1\underline{L}$ state to the $5p^5 4f^1$ state; this strong coupling transfers $5p^5 4f^1$ character to peak B. Feature C (yellow-shaded region) at 18–24 eV energy transfer stands for the atomic multiplets of the La $5p^5 4f^1$ final state.[42,57] Here, the RIXS symmetry selection rule gives access to four multiplet final states ($^3D_1$, $^3D_2$, $^3F_2$, and $^1D_2$ (Figure 2d). Those are a subset of the 12 discrete states that the La $5p^5 4f^1$ electronic configuration allows for in the free ion $J_1 l$ coupling scheme.[61] However, six states thereof have been identified using the sliding spark technique[61] with significant deviation from pure $J_1 l$ coupling due to the 4f contraction and concomitant 5p–4f orbital interaction. In a nutshell, all levels are of mixed nature except for the energetically lowest $^3D_1$ state. For this reason, we base all further analysis on the La $5p^5 4f^1$ $^3D_1$ RIXS final state shown in Figure 2e, since the high spectral resolution[52] allows us to distinguish the $^3D_1$ and $^3D_2$ contributions, which were inseparable in previous work.[42,57]

https://doi.org/10.1021/acs.jpcc.3c02011
J. Phys. Chem. C 2023, 127, 11111−11118

We also note that the excitonic nature has been evidenced earlier by detuning experiments which prove the peaks we are observing are constant-loss features.[57]

Figure 3a shows the experimental RIXS data of the La $5p^54f^1$ $^3D_1$ and $^3D_2$ final states of lanthanum metal, La_2O_3, $SrLaAlO_4$, $LaAlO_3$, $LaPO_4$:Ce,Tb, and LaF_3 measured with unprecedented subnatural line width spectral resolution of 45−60 meV at the meV-RIXS experimental station of BESSY II.[52] Gradual shift of the leading edge and different broadening are observed. As XAS and RIXS both possess charge-neutral final states, the peak broadening and energy shift must stem from chemical sensitivity. If we simply fix the Gaussian parameters to the spectral resolution and fit all the RIXS spectra with two Voigt profiles, inconsistent energy separation and relative intensities are found in the fitted result. It indicates in some samples, especially non-single crystal ones, the broadening is rather governed by the chemical broadening instead of intrinsic lifetime and instrumental broadening. We first fit the $^3D_1$ and $^3D_2$ peaks from single crystal $LaAlO_3$ by two Voigt profiles with Gaussian parameters fixed to spectral resolution, and the other parameters are set free (Figure 2e). We extract the energy position separation (0.212 eV), relative intensity ratio (1.016:1), and Lorentzian parameters (γ_{D1} = 0.103 eV, γ_{D2} = 0.169 eV) of the two peaks and define this as our empirical model. We then apply this model to fit all samples by fixing the energy separation, relative intensity ratio, and Lorentzian parameters, and we constrain the Gaussian parameters to be coupled between $^3D_1$ and $^3D_2$ peaks. This stringent model has the physical meaning that the atomic nature is conserved and both peaks have identical isotropic chemical broadening. At first glance of the fitted results (Figure S2, Table S1), it is clear that only single crystal samples possess the well-defined atomic-like lineshapes. The other samples are having more or less different degrees of chemical broadening. Chemical inhomogeneity leads to multiple shifted features and gives rise to a single composite feature. Using the same fitting strategy with fixed Gaussian to spectral resolution and coupled Lorentzian as free parameter, on the other hand, does not capture the line shape better (Figure S3, Table S2), which suggests that lifetime is less likely to be the dominant broadening mechanism.

The only discrepancy of our empirical model was found in LaF_3, where the energy separation needs to be reduced to better capture the line shape. We attribute the smaller energy separation to different Slater integral, which originates from different Coulomb interaction, partially from nephelauxetic effect, between LaF_3 and $LaAlO_3$.

Since $^3D_1$ is the lowest in energy and is the only pure state in $5p^54f^1$ configuration, we define the upper boundary of the $^3D_1$ state by fitting all spectra to unconstrained single Voigt. The single Voigt peak center is always greater than or equal to the RIXS peak maximum. The lower boundary is then defined by the leading-edge fit, where we select the lowest limit from either fixed-Gaussian or fixed-Lorentzian model described earlier. We then define the two boundaries as the uncertainty region in energy position. The fixed-Lorentzian fitted La $5p^54f^1$ $^3D_1$ peak positions and the boundaries are summarized in Table 1 and put into perspective with the reported band gap values of the respective materials. The data and uncertainty region from Table 1 are displayed in Figure 3b. We note that the error bar indicates the uncertainty we defined earlier but not the standard error.

Table 1. Fitted Result of La $5p^54f^1$ $^3D_1$ Peak Positions (Based on Fixed Lorentzian Parameters), Estimated Uncertainty Region, and Band Gap Energies

sample	$^3D_1$ center (eV)	upper boundary (eV)	lower boundary (eV)	band gap (eV)
La metal	18.62	18.71	18.59	0
La_2O_3	18.72	18.81	18.69	4.3[62]
$SrLaAlO_4$	18.86	18.92	18.83	5[63]
$LaAlO_3$	18.96	19.03	18.93	5.6[64]
$LaPO_4$:Ce,Tb	19.38	19.47	19.36	8[65]
LaF_3	19.44	19.48	19.42	9.7[66]

We observe a gradual increase of the La $5p^54f^1$ $^3D_1$ final state energy transfer in the spectra with increasing band gap energy of the materials. This suggests the general observation that the chemical sensitivity of the La $5p^54f^1$ $^3D_1$ final state energy might trace covalency or electronegativity. First of all, we identify three regions depending on bonding type (local) and band gap (global) shown in Figure 3b: the metallic lanthanum (red-shaded, no band gap), the highly ionic LaF_3 (blue-shaded, band gap = 9.7 eV), and the mixed-covalent-ionic simple oxides and phosphates (green-shaded, band gap = 2−8 eV). The La $5p^54f^1$ $^3D_1$ resonantly excited RIXS final state is charge balanced as is the ground state. Thus, all variations in the final state energy stem from accommodating the localized $4f^1$ charge involving strongly the $5p^5$ electrons that are influenced in a varying degree of covalency with the host material. In lanthanum metal, even the $5d^16s^2$ valence electrons contribute, leading to the lowest observed La $5p^54f^1$ $^3D_1$ final state energy. The insulating materials are lacking these mobile electrons, which results in an offset of the final state energy scale. Within this line of reasoning the highly ionic LaF_3 salt, caused by the high fluoride electronegativity, reduces the charge density at the metal center. This is reflected in the highest La $5p^54f^1$ $^3D_1$ final state energy of the series. The chemical shift seen in 5p hence indicates the degree of covalency. Even though it is difficult to differentiate the contribution from direct 5p bonding and hybridization (with 5d/6s)-mediated covalent bonding, effectively the covalency influences the 5p RIXS energy position.

From 3d XPS[32] we know that the ground state in La_2O_3 is $4f^0 + 4f^1\underline{L}$ with charge transfer Δ = 12.5 eV, yielding the $4f^1\underline{L}$ antibonding peak at 12 eV. Similarly, the intermediate state is $4d^94f^1 + 4d^94f^2\underline{L}$, with similar Δ, which implies that the $4d^94f^1$ is again more than 99% pure. One would then also expect that the $5p^54f^1$ will be more than 99% pure, but several mechanisms will create a mixing of states. The $5p^54f^1$ has large multipet splitting, implying that the highest multiplet states of $5p^54f^1$ overlap with the lowest multiplet states of $5p^54f^2\underline{L}$. This will mainly affect the highest multiplet $^1D_2$ state (Figure 2d), as is visible in the experiments. There are other charge transfer mechanisms at play, including the mixing with $4f^1\underline{L}$ (creating peak B) and the charge transfer of the 5d and valence electrons, where we note that these charge transfer effects will become stronger when the band gap gets smaller.

We further link the local excitation process to the global band structure: the mixed-covalent-ionic simple oxides and phosphate show a linear dependence of La $5p^54f^1$ $^3D_1$ final state energy with the band gap reflecting a decreased charge sharing toward larger band gaps. From a beyond-local perspective, "larger band gap, weaker screening" is the general

https://doi.org/10.1021/acs.jpcc.3c02011
J. Phys. Chem. C 2023, 127, 11111−11118

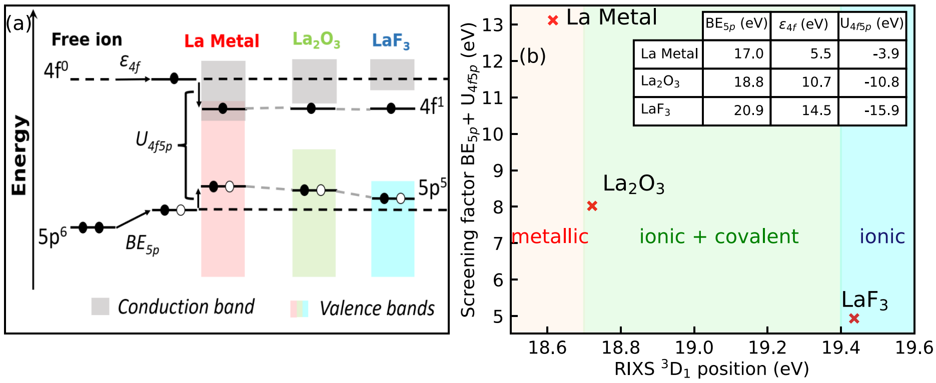

Figure 4. (a) Scheme and energies of the screened $5p^5$ hole, the $4f^1$ electron, and the $5p^54f^1$ Coulomb attraction embedded to the lanthanum metal, the mixed-covalent-ionic La_2O_3 solid, and the highly ionic LaF_3 salt. The atomic localized 4f level defines a natural reference level. (b) Tabulated values of BE_{5p}: $5p^5$ hole state binding energy, ϵ_{4f}, $4f^1$ electron orbital energy and the additional U_{4f5p} Coulomb attraction of the screened $5p^5$ hole with the screened $4f^1$ electron. The graph shows the apparent screening factor with the $4f^1$ as an atomic reference level for the lanthanum metal, the mixed-covalent-ionic La_2O_3, and the highly ionic LaF_3 salt.

concept for exciton which might link to the universal scaling established earlier in 2D semiconducting systems.[67,68]

Further analysis is performed by assuming a fully localized 4f level, and we set 4f as our reference state. The assumption is based on our XAS data where no hints of chemical sensitivity were observed. Previous reports also stated that the perturbation of 4f level,[69−71] which can be understood under the nephelauxetic effect, is at least an order of magnitude smaller in comparison to the ≈0.9 eV chemical shift observed in our RIXS data. Hence, we can also see the lanthanum $5p^54f^1$ $^3D_1$ final state as a sensor of the 5p sharing within the host lattice, which means 5p is the leading term. In the following and as a further step, we show how to assess the energies of the $5p^5$ hole and the $4f^1$ electron independently and then extract the excitonic electron−hole Coulomb attraction as well as the screening factor. Let us derive these energies for the lanthanum metal, the mixed-covalent-ionic La_2O_3 and the highly ionic LaF_3 salt as shown in Figure 4a. In a single electron picture, the measured RIXS excitonic $5p^54f^1$ final state energy can be expressed as $E_{RIXS(5p4f)} = BE_{5p} + \epsilon_{4f} + U_{4f5p}$, where BE_{5p} is the single hole $5p^5$ electron binding energy, ϵ_{4f} is the singly occupied $4f^1$ orbital energy, and U_{4f5p} stands for the Coulomb attraction between the $4f^1$ electron and the $5p^5$ hole.[59]

For lanthanum metal, mixed-covalent-ionic La_2O_3 and ionic LaF_3 salt, the $5p^5$ electron binding energies are readily available from photoemission data[72] and tabulated within Figure 4b. So are the $4f^1$ ϵ_{4f} values from X-ray photoelectron spectroscopy (XPS), electron energy loss spectroscopy (EELS), and Bremsstrahlung isochromat spectroscopy (BIS).[73] Although the character of the host material changes from metallic to ionic, the La $5p^5$ hole energy BE_{5p} changes only a few eV, whereas the $4f^1$ ϵ_{4f} orbital energy varies by almost 10 eV. Effectively, the atomic localization of the $4f^1$ electron vs the partially shared nature of the $5p^5$ hole within the La 5p shell makes the $4f^1$ electron apparently experience a relatively stronger intra- and interatomic relaxation and screening in the respective host materials in comparison to the free ion. The screening itself varies from metallic to dipolar or charge transfer screening. Most notable, the screening of the $5p^5$ hole and of the $4f^1$ electron still leaves room for the attractive Coulomb interaction between the already screened $5p^5$ hole and the screened $4f^1$ electron, leading to the excitonic La $5p^54f^1$ $^3D_1$ final state energy $E_{RIXS(5p4f)}$ measured in our RIXS experiment. Thus, our measurements allow extracting the attractive Coulomb interaction energy between the screened $5p^5$ hole and the screened $4f^1$ electron $U_{4f5p} = E_{RIXS(5p4f)} - \epsilon_{4f} - BE_{5p}$. We note that even in the metallic lanthanum, the atomic nature of the screened $4f^1$ electron must be maintained by additional Coulomb attraction to the 5p charges, and thus a sizable excitonic Coulomb energy U_{4f5p} of approximately −4 eV occurs. Let us finally take the localized $4f^1$ state as a natural reference level and plot in Figure 4b the apparent screening factor $BE_{5p} + U_{4f5p}$, in which the local and nonlocal screening are captured. The metal has the best screening, whereas in oxides the hole is partially screened via covalent interaction. The highly electronegative F^- withdraws the charge in its ionic lattice and hence prohibits electron sharing. Since all La-based compounds share the same $5p^54f^1$ final state, our RIXS data are consistent with the independent spectroscopic methods.

We can now utilize our established sensitivity of La 5p by looking at the changes in delocalization undergoing geometrical quantum confinement.[2,74,75] By keeping the bond length, coordination, and local geometry equivalent in $LaPO_4$, namely, monoclinic structure, we prepared 0D, 1D nanostructure and bulk samples: $LaPO_4$:Ce,Tb quantum dots (QD), $LaPO_4$ quantum wires (QW), and bulk-like $LaPO_4$ microcrystals. Diffuse reflectance spectroscopy (DRS) measurements (Figure S7) show confinement for the nanoscale objects, and only the bulk samples possess clear band-like absorption in the lower energy window. Figure 5 contains the La $5p^54f^1$ $^3D_{1,2}$ final states RIXS spectra and peak positions in direct comparison for the bulk-like microcrystals without quantum confinement (microrod, 3D electron system), the 4 nm nanoparticles with quantum confinement in all dimensions (quantum dot, 0D electron system), and the 30 nm long nanowire structures with confinement in two directions (quantum wire, 1D electron system). We observe how increased quantum confinement shifts the La $5p^54f^1$ $^3D_{1,2}$ final state energy to higher transfer energies in comparison to the bulk-like microcrystals. We note that the La $5p^54f^1$ $^3D_{1,2}$ final-state spectrum of the 30 nm quantum wire shows signs of both confinement and bulk-like properties in its spectral shape. This reflects the fact that depending on the relative spatial orientation to the geometric shape, two dimensions are confined, whereas the direction along the quantum wire remains unconfined. Hence the RIXS spectrum captures even the anisotropy of the confinement and the valence electron

https://doi.org/10.1021/acs.jpcc.3c02011
J. Phys. Chem. C 2023, 127, 11111−11118

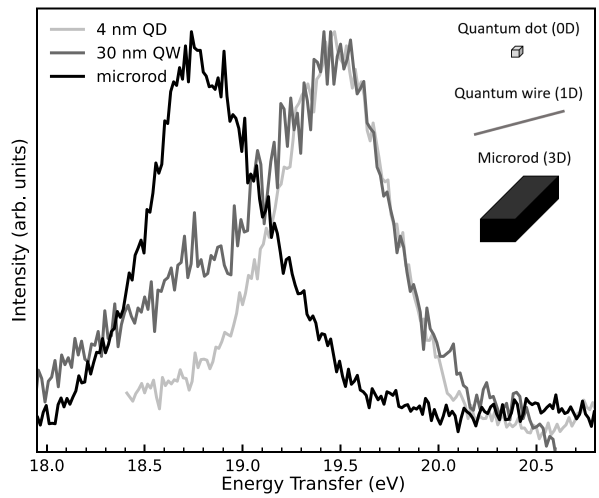

Figure 5. RIXS spectra of the La $5p^54f^1$ $^3D_{1,2}$ final states of the mixed-covalent-ionic $LaPO_4$ quantum dot (QD), quantum wire (QW), and bulk-like microrods. Sensitivity to the modified 5p sharing from geometric constraint occurs despite the identical local bonding within the base material $LaPO_4$. Note the presence of quantum-confined and bulk-like features in the geometrically anisotropically confined quantum wires.

sharing within the quantum wire structure. Based on the $LaPO_4$ confinement study in charge-neutral well-screened RIXS final states, we can thus differentiate band-like and free-ion-like La, which is consistent with the benchmark materials.

■ CONCLUSION

We demonstrate the use of La 5p as covalency descriptor in RIXS experiments. With help of unprecedented spectral resolution, we establish an empirical model from single crystal $LaAlO_3$ and use this model to determine the La $5p^54f^1$ $^3D_1$ RIXS final state energy positions in benchmark samples. The La $5p^54f^1$ $^3D_1$ RIXS final state exists for all host materials alike, but its energy is highly sensitive to the screening environment and the degree of covalency. As a result, the La 5p can serve as atomic sensor and differentiate band-like and free-ion-like La between La metal, mixed-covalent-ionic La^{3+} simple oxides and phosphates as well as highly ionic LaF_3 salt. The excitonic character of the La $5p^54f^1$ $^3D_1$ RIXS final state also allows us to verify our established relationship in an impurity model to independent relaxation energies of the La $5p^5$ hole state, the La $4f^1$ electron, and the $5p^54f^1$ Coulomb attraction from XPS, EELS, and BIS measurements. Finally, we apply our technique to visualize quantum confinement and its geometric anisotropy with regard to valence electron sharing in mixed-covalent-ionic $LaPO_4$.

■ ASSOCIATED CONTENT

Supporting Information

The Supporting Information is available free of charge at https://pubs.acs.org/doi/10.1021/acs.jpcc.3c02011.

XAS data of all samples, detailed fitted RIXS and their parameters, characterization of the nanomaterials, and DRS spectra (PDF)

■ AUTHOR INFORMATION

Corresponding Authors

Chun-Yu Liu − *Institute for Methods and Instrumentation for Synchrotron Radiation Research (PS-ISRR), Helmholtz-Zentrum Berlin für Materialien und Energie GmbH, 12489 Berlin, Germany; Institute of Physics and Astronomy, University of Potsdam, 14476 Potsdam, Germany;* orcid.org/0000-0003-4385-9328; Email: chun-yu.liu@helmholtz-berlin.de

Alexander Föhlisch − *Institute for Methods and Instrumentation for Synchrotron Radiation Research (PS-ISRR), Helmholtz-Zentrum Berlin für Materialien und Energie GmbH, 12489 Berlin, Germany; Institute of Physics and Astronomy, University of Potsdam, 14476 Potsdam, Germany;* orcid.org/0000-0003-4126-8233; Email: alexander.foehlisch@helmholtz-berlin.de

Authors

Ping Feng − *Department for Electrochemical Energy Storage, Helmholtz-Zentrum Berlin für Materialien und Energie, 14109 Berlin, Germany; Institute of Chemistry, University of Potsdam, Potsdam 14476, Germany*

Kari Ruotsalainen − *Institute for Methods and Instrumentation for Synchrotron Radiation Research (PS-ISRR), Helmholtz-Zentrum Berlin für Materialien und Energie GmbH, 12489 Berlin, Germany*

Karl Bauer − *Institute for Methods and Instrumentation for Synchrotron Radiation Research (PS-ISRR), Helmholtz-Zentrum Berlin für Materialien und Energie GmbH, 12489 Berlin, Germany;* orcid.org/0000-0003-0664-2082

Régis Decker − *Institute for Methods and Instrumentation for Synchrotron Radiation Research (PS-ISRR), Helmholtz-Zentrum Berlin für Materialien und Energie GmbH, 12489 Berlin, Germany*

Maximilian Kusch − *Institute for Methods and Instrumentation for Synchrotron Radiation Research (PS-ISRR), Helmholtz-Zentrum Berlin für Materialien und Energie GmbH, 12489 Berlin, Germany*

Katarzyna E. Siewierska − *Institute for Methods and Instrumentation for Synchrotron Radiation Research (PS-ISRR), Helmholtz-Zentrum Berlin für Materialien und Energie GmbH, 12489 Berlin, Germany*

Annette Pietzsch − *Institute for Methods and Instrumentation for Synchrotron Radiation Research (PS-ISRR), Helmholtz-Zentrum Berlin für Materialien und Energie GmbH, 12489 Berlin, Germany*

Markus Haase − *Department of Inorganic Chemistry, Functional Nanomaterials, University of Osnabrück, Osnabrück 49074, Germany;* orcid.org/0000-0002-9686-8810

Yan Lu − *Department for Electrochemical Energy Storage, Helmholtz-Zentrum Berlin für Materialien und Energie, 14109 Berlin, Germany; Institute of Chemistry, University of Potsdam, Potsdam 14476, Germany;* orcid.org/0000-0003-3055-0073

Frank M. F. de Groot − *Department of Chemistry, Utrecht University, 3584 CC Utrecht, The Netherlands;* orcid.org/0000-0002-1340-2186

Complete contact information is available at: https://pubs.acs.org/10.1021/acs.jpcc.3c02011

Notes

The authors declare no competing financial interest.

■ ACKNOWLEDGMENTS

We acknowledge Dr. Galina Gurieva for providing support in DRS measurements.

■ REFERENCES

(1) Joos, J. J.; Poelman, D.; Smet, P. F. Energy Level Modeling of Lanthanide Materials: Review and Uncertainty Analysis. *Phys. Chem. Chem. Phys.* **2015**, *17*, 19058−19078.

(2) Klein, J.; Beladi-Mousavi, S. M.; Schleutker, M.; Taffa, D. H.; Haase, M.; Walder, L. Photo-Electrochemical Device Enabling Luminescence Switching of $LaPO_4$:Ce,Tb Nanoparticle Layers. *Adv. Opt. Mater.* **2021**, *9*, 2001891.

(3) Li, L.; Li, T.; Hu, Y.; Cai, C.; Li, Y.; Zhang, X.; Liang, B.; Yang, Y.; Qiu, J. Mechanism of the Trivalent Lanthanides' Persistent Luminescence in Wide Bandgap Materials. *Light Sci. Appl.* **2022**, *11*, 51.

(4) Menge, P. R.; Gautier, G.; Iltis, A.; Rozsa, C.; Solovyev, V. Performance of Large Lanthanum Bromide Scintillators. *Nucl. Instruments Methods Phys. Res. Sect. A Accel. Spectrometers, Detect. Assoc. Equip.* **2007**, *579*, 6−10.

(5) Chattopadhyay, D.; Sharma, S.; Sarkar, M. S. Reduction of the Effect of Internal Activity in $LaCl_3$:Ce Scintillator. *J. Instrum.* **2021**, *16*, P06025.

(6) Drozdov, A. P.; Kong, P. P.; Minkov, V. S.; Besedin, S. P.; Kuzovnikov, M. A.; Mozaffari, S.; Balicas, L.; Balakirev, F. F.; Graf, D. E.; Prakapenka, V. B.; et al. Superconductivity at 250 K in Lanthanum Hydride Under High Pressures. *Nature* **2019**, *569*, 528−531.

(7) Li, D.; Lee, K.; Wang, B. Y.; Osada, M.; Crossley, S.; Lee, H. R.; Cui, Y.; Hikita, Y.; Hwang, H. Y. Superconductivity in an Infinite-Layer Nickelate. *Nature* **2019**, *572*, 624−627.

(8) Morris, R. C.; Cline, C. F.; Begley, R. F.; Dutoit, M.; Harget, P. J.; Jenssen, H. P.; La France, T. S.; Webb, R. Lanthanum Beryllate: A New Rare-Earth Ion Laser Host. *Appl. Phys. Lett.* **1975**, *27*, 444.

(9) Aminoff, C.; Larat, C.; Leduc, M.; Viana, B.; Vivien, D. Characterization and Laser Properties of Lanthanum Magnesium Hexa-Aluminate Activated by Neodymium and Chromium. *J. Lumin.* **1991**, *50*, 21−29.

(10) Malacrida, P.; Escudero-Escribano, M.; Verdaguer-Casadevall, A.; Stephens, I. E.; Chorkendorff, I. Enhanced Activity and Stability of Pt-La and Pt-Ce Alloys for Oxygen Electroreduction: The Elucidation of the Active Surface Phase. *J. Mater. Chem. A* **2014**, *2*, 4234−4243.

(11) Zhu, H.; Zhang, P.; Dai, S. Recent Advances of Lanthanum-Based Perovskite Oxides for Catalysis. *ACS Catal.* **2015**, *5*, 6370−6385.

(12) Dervishogullari, D.; Sharpe, C. A.; Sharpe, L. R. $LaFe_xCo_{(1-x)}O_3$ Thin-Film Oxygen Reduction Catalysts Prepared Using Spray Pyrolysis Without Conductive Additives. *ACS Omega* **2017**, *2*, 7695−7701.

(13) Baeumer, C.; Li, J.; Lu, Q.; Liang, A. Y. L.; Jin, L.; Martins, H. P.; Duchoň, T.; Glöß, M.; Gericke, S. M.; Wohlgemuth, M. A.; et al. Tuning Electrochemically Driven Surface Transformation in Atomically Flat $LaNiO_3$ Thin Films for Enhanced Water Electrolysis. *Nat. Mater.* **2021**, *20*, 674−682.

(14) Xu, J.; Chen, X.; Xu, Y.; Du, Y.; Yan, C. Ultrathin 2D Rare-Earth Nanomaterials: Compositions, Syntheses, and Applications. *Adv. Mater.* **2020**, *32*, 1806461.

(15) Löble, M. W.; Keith, J. M.; Altman, A. B.; Stieber, S. C. E.; Batista, E. R.; Boland, K. S.; Conradson, S. D.; Clark, D. L.; Lezama Pacheco, J.; Kozimor, S. A.; et al. Covalency in Lanthanides. An X-Ray Absorption Spectroscopy and Density Functional Theory Study of $LnCl_6^{x-}$(X = 3, 2). *J. Am. Chem. Soc.* **2015**, *137*, 2506−2523.

(16) Kvashnina, K. O.; Butorin, S. M.; Glatzel, P. Direct Study of the F-Electron Configuration in Lanthanide Systems. *J. Anal. At. Spectrom.* **2011**, *26*, 1265−1272.

(17) Kotani, A.; Shin, S. Resonant Inelastic X-Ray Scattering Spectra for Electrons in Solids. *Rev. Mod. Phys.* **2001**, *73*, 203−246.

(18) Shen, J. X.; Schleife, A.; Janotti, A.; Van De Walle, C. G. Effects of La 5d and 4f States on the Electronic and Optical Properties of $LaAlO_3$. *Phys. Rev. B* **2016**, *94*, 205203.

(19) Yang, J.; Dolg, M. Valence Basis Sets for Lanthanide 4f-in-Core Pseudopotentials Adapted for Crystal Orbital Ab Initio Calculations. *Theor. Chem. Acc.* **2005**, *113*, 212−224.

(20) Vitova, T.; Pidchenko, I.; Fellhauer, D.; Bagus, P. S.; Joly, Y.; Pruessmann, T.; Bahl, S.; Gonzalez-Robles, E.; Rothe, J.; Altmaier, M.; et al. The Role of the 5f Valence Orbitals of Early Actinides in Chemical Bonding. *Nat. Commun.* **2017**, *8*, 16053.

(21) Butorin, S. M.; Kvashnina, K. O.; Vegelius, J. R.; Meyer, D.; Shuh, D. K. High-Resolution X-Ray Absorption Spectroscopy as a Probe of Crystal-Field and Covalency Effects in Actinide Compounds. *Proc. Natl. Acad. Sci. U. S. A.* **2016**, *113*, 8093−8097.

(22) Zhang, Y.; Duan, W.; Yang, Y.; Jian, T.; Qiao, Y.; Ren, G.; Zhang, N.; Zheng, L.; Yan, W.; Wang, J.; et al. Involvement of 5f Orbitals in the Covalent Bonding Between the Uranyl Ion and Trialkyl Phosphine Oxide: Unraveled by Oxygen K-Edge X-Ray Absorption Spectroscopy and Density Functional Theory. *Inorg. Chem.* **2022**, *61*, 92−104.

(23) Kvashnina, K. O.; Butorin, S. M. High-Energy Resolution X-Ray Spectroscopy at Actinide $M_{4,5}$ and Ligand K Edges: What We Know, What We Want to Know, and What We Can Know. *Chem. Commun.* **2022**, *58*, 327−342.

(24) Gu, Y.; Zhu, S.; Wang, X.; Hu, J.; Chen, H. A Substantial Hybridization Between Correlated Ni-d Orbital and Itinerant Electrons in Infinite-Layer Nickelates. *Commun. Phys.* **2020**, *3*, 84.

(25) Hepting, M.; Li, D.; Jia, C. J.; Lu, H.; Paris, E.; Tseng, Y.; Feng, X.; Osada, M.; Been, E.; Hikita, Y.; et al. Electronic Structure of the Parent Compound of Superconducting Infinite-Layer Nickelates. *Nat. Mater.* **2020**, *19*, 381−385.

(26) Rossi, M.; Osada, M.; Choi, J.; Agrestini, S.; Jost, D.; Lee, Y.; Lu, H.; Wang, B. Y.; Lee, K.; Nag, A.; et al. A Broken Translational Symmetry State in an Infinite-Layer Nickelate. *Nat. Phys.* **2022**, *18*, 869−873.

(27) Smiles, D. E.; Batista, E. R.; Booth, C. H.; Clark, D. L.; Keith, J. M.; Kozimor, S. A.; Martin, R. L.; Minasian, S. G.; Shuh, D. K.; Stieber, S. C. E.; et al. The Duality of Electron Localization and Covalency in Lanthanide and Actinide Metallocenes. *Chem. Sci.* **2020**, *11*, 2796−2809.

(28) Vitova, T.; Roesky, P. W.; Dehnen, S. Open Questions on Bonding Involving Lanthanide Atoms. *Commun. Chem.* **2022**, *5*, 12.

(29) Rivera, V.; Ferri, F., Marega, E., Jr. In *Plasmonics—Principles and Applications*; Kim, K. Y., Ed.; IntechOpen: Rijeka, Croatia, 2012; Chapter 11.

(30) Temmerman, W.; Petit, L.; Svane, A.; Szotek, Z.; Lüders, M.; Strange, P.; Staunton, J.; Hughes, I.; Gyorffy, B. The Dual, Localized or Band-like, Character of the 4f-States; *Handbook on the Physics and Chemistry of Rare Earths*; Elsevier, 2009; Vol. *39*; Chapter 241, pp 1−112.

(31) Dorenbos, P. The Nephelauxetic Effect on the Electron Binding Energy in the $4f^q$ Ground State of Lanthanides in Compounds. *J. Lumin.* **2019**, *214*, 116536.

(32) Kotani, A.; Ogasawara, H. Theory of Core-Level Spectroscopy of Rare-Earth Oxides. *J. Electron Spectrosc. Relat. Phenom.* **1992**, *60*, 257−299.

(33) Yu, S. W.; Carpenter, M. H.; Ponce, F.; Friedrich, S.; Lee, J. S. Atomic Origin of $3d^94f^1$ Configuration in La^{3+} Solids. *J. Phys.: Condens. Matter* **2015**, *27*, 405501.

(34) Ji, W.-X.; Xu, W.; Xiao, Y.; Wang, S.-G. Does the 4f-Shell Contribute to Bonding in Tetravalent Lanthanide Halides? *J. Chem. Phys.* **2014**, *141*, 244316.

(35) Maslakov, K. I.; Teterin, Y. A.; Ryzhkov, M. V.; Popel, A. J.; Teterin, A. Y.; Ivanov, K. E.; Kalmykov, S. N.; Petrov, V. G.; Petrov, P. K.; Farnan, I. The Electronic Structure and the Nature of the Chemical Bond in CeO_2. *Phys. Chem. Chem. Phys.* **2018**, *20*, 16167−16175.

(36) Minasian, S. G.; Batista, E. R.; Booth, C. H.; Clark, D. L.; Keith, J. M.; Kozimor, S. A.; Lukens, W. W.; Martin, R. L.; Shuh, D. K.;

Stieber, S. C. E.; et al. Quantitative Evidence for Lanthanide-Oxygen Orbital Mixing in CeO_2, PrO_2, and TbO_2. *J. Am. Chem. Soc.* **2017**, *139*, 18052−18064.
(37) Fisk, Z.; Sarrao, J. L.; Smith, J. L.; Thompson, J. D. The Physics and Chemistry of Heavy Fermions. *Proc. Natl. Acad. Sci. U. S. A.* **1995**, *92*, 6663−6667.
(38) Choi, H. C.; Min, B. I.; Shim, J. H.; Haule, K.; Kotliar, G. Temperature-Dependent Fermi Surface Evolution in Heavy Fermion $CeIrIn_5$. *Phys. Rev. Lett.* **2012**, *108*, 016402.
(39) Denning, R. G.; Harmer, J.; Green, J. C.; Irwin, M. Covalency in the 4f Shell of *tris*-Cyclopentadienyl Ytterbium ($YbCp_3$)- A Spectroscopic Evaluation. *J. Am. Chem. Soc.* **2011**, *133*, 20644−20660.
(40) Krogh-Jespersen, K.; Romanelli, M. D.; Melman, J. H.; Emge, T. J.; Brennan, J. G. Covalent Bonding and the Trans Influence in Lanthanide Compounds. *Inorg. Chem.* **2010**, *49*, 552−560.
(41) Xu, W.; Ji, W. X.; Qiu, Y. X.; Schwarz, W. H.; Wang, S. G. On Structure and Bonding of Lanthanoid Trifluorides LnF_3 (Ln = La to Lu). *Phys. Chem. Chem. Phys.* **2013**, *15*, 7839−7847.
(42) Moewes, A.; Postnikov, A. V.; Kurmaev, E. Z.; Grush, M. M.; Ederer, D. L. Resonant Mixing of Widely Separated Intermediate States and Charge Transfer at the 4d-4f Resonance of La Compounds. *Europhys. Lett.* **2000**, *49*, 665−671.
(43) Lu, J. B.; Jiang, X. L.; Hu, H. S.; Li, J. Norm-Conserving 4f-in-Core Pseudopotentials and Basis Sets Optimized for Trivalent Lanthanides (Ln = Ce-Lu). *J. Chem. Theory Comput.* **2023**, *19*, 82−96.
(44) Teterin, Y.; Teterin, A.; Utkin, I.; Ryzhkov, M. XPS study of the Ln 5p,4f-electronic states of lanthanides in Ln2O3. *J. Electron Spectrosc. Relat. Phenom.* **2004**, *137−140*, 601−605. ICESS-9 Proceedings of the 9th International Conference on Electronic Spectroscopy and Structure.
(45) Blyth, R. I.; Patchett, A. J.; Dhesi, S. S.; Cosso, R.; Barrett, S. D. Band Effects in the 5p Levels of Ho(0001). *J. Phys.: Condens. Matter* **1991**, *3*, S287.
(46) Aravena, D.; Neese, F.; Pantazis, D. A. Improved Segmented All-Electron Relativistically Contracted Basis Sets for the Lanthanides. *J. Chem. Theory Comput.* **2016**, *12*, 1148−1156.
(47) Lu, T.; Chen, F. Multiwfn: A Multifunctional Wavefunction Analyzer. *J. Comput. Chem.* **2012**, *33*, 580−592.
(48) Ament, L. J.; Van Veenendaal, M.; Devereaux, T. P.; Hill, J. P.; Van Den Brink, J. Resonant Inelastic X-Ray Scattering Studies of Elementary Excitations. *Rev. Mod. Phys.* **2011**, *83*, 705−767.
(49) Gel'mukhanov, F.; Odelius, M.; Polyutov, S. P.; Föhlisch, A.; Kimberg, V. Dynamics of Resonant X-ray and Auger Scattering. *Rev. Mod. Phys.* **2021**, *93*, 035001.
(50) Kachel, T. The Plane Grating Monochromator Beamline U49-2 PGM-1 at BESSY II. *J. Large-Scale Res. Facil.* **2016**, *2*, A72.
(51) Beye, M.; Miedema, P. S. Solid flexRIXS: A RIXS Endstation for Solid Systems at BESSY II. *J. Large-Scale Res. Facil.* **2017**, *3*, A124.
(52) Bauer, K.; Schmidt, J.-S.; Eggenstein, F.; Decker, R.; Ruotsalainen, K.; Pietzsch, A.; Blume, T.; Liu, C.-Y.; Weniger, C.; Siewert, F.; et al. The meV XUV-RIXS Facility at UE112-PGM1 of BESSY II. *J. Synchrotron Radiat.* **2022**, *29*, 908.
(53) Riwotzki, K.; Meyssamy, H.; Kornowski, A.; Haase, M. Liquid-Phase Synthesis of Doped Nanoparticles: Colloids of Luminescing $LaPO_4$:Eu and $CePO_4$:Tb Particles With a Narrow Particle Size Distribution. *J. Phys. Chem. B* **2000**, *104*, 2824−2828.
(54) Wang, K.; Yao, W.; Teng, F.; Zhu, Y. Photocatalytic Activity Enhancement of $LaPO_4$ via Surface Oxygen Vacancies. *RSC Adv.* **2015**, *5*, 56711−56716.
(55) Miyahara, T.; Hanyu, T.; Ishii, H.; Yanagihara, M.; Kamada, T.; Kato, H.; Naito, K.; Suzuki, S. The 4d Photoabsorption Spectra of La, LaF_3, Ba and BaF_2: Dependence on the Chemical and Structural Environment. *J. Phys. Soc. Jpn.* **1986**, *55*, 408−413.
(56) Aono, M.; Chiang, T. C.; Knapp, J. A.; Tanaka, T.; Eastman, D. E. Direct Recombination and Auger Deexcitation Channels of La 4*d* → 4*f* Resonant Excitations in LaB_6. *Phys. Rev. B* **1980**, *21*, 2661−2665.
(57) Suljoti, E.; de Groot, F. M. F.; Nagasono, M.; Glatzel, P.; Hennies, F.; Deppe, M.; Pietzsch, A.; Sonntag, B.; Föhlisch, A.; Wurth, W. Spin-Orbit Mediated Interference in the Radiative and Nonradiative Channels of the La 4*d* Core Resonances. *Phys. Rev. Lett.* **2009**, *103*, 137401.
(58) Dehmer, J. L.; Starace, A. F.; Fano, U.; Sugar, J.; Cooper, J. W. Raising of Discrete Levels Into the Far Continuum. *Phys. Rev. Lett.* **1971**, *26*, 1521−1525.
(59) Miller, T.; Chiang, T.-C. Solid-state Screening Effect on the Post-collision Interaction. *Phys. Rev. B* **1984**, *29*, 1121−1124.
(60) Suzuki, S.; Ishii, T.; Sagawa, T. 4d-Shell Photoabsorption Spectra of Lanthanum- and Cerium-Halides. *J. Phys. Soc. Jpn.* **1975**, *38*, 156−161.
(61) Epstein, G. L.; Reader, J. Spectrum and Energy Levels of Triply Ionized Lanthanum (La Iv). *J. Opt. Soc. Am.* **1979**, *69*, 511.
(62) Ravi, G.; Sarasija, M.; Ayodhya, D.; Kumari, L. S.; Ashok, D. Facile Synthesis, Characterization and Enhanced Catalytic Reduction of 4-Nitrophenol Using NaBH4 by Undoped and Sm^{3+}, Gd^{3+}, Hf^{3+} Doped La_2O_3 Nanoparticles. *Nano Convergence* **2019**, *6*, 12.
(63) Devi, S.; Khatkar, A.; Taxak, V.; Hooda, A.; Sehrawat, P.; Singh, S.; Khatkar, S. Influence of Tb^{3+} Doping on the Structural and Down-conversion Luminescence Behaviour of $SrLaAlO_4$ Nanophosphor. *J. Lumin.* **2020**, *221*, 117064.
(64) Yoshimatsu, K.; Yasuhara, R.; Kumigashira, H.; Oshima, M. Origin of Metallic States at the Heterointerface between the Band Insulators $LaAlO_3$ and $SrTiO_3$. *Phys. Rev. Lett.* **2008**, *101*, 026802.
(65) Pankratov, V.; Popov, A. I.; Shirmane, L.; Kotlov, A.; Feldmann, C. $LaPO_4$:Ce,Tb and YVO_4:Eu Nanophosphors: Luminescence Studies in the Vacuum Ultraviolet Spectral Range. *J. Appl. Phys.* **2011**, *110*, 053522.
(66) Wiemhöfer, H. D.; Harke, S.; Vohrer, U. Electronic Properties and Gas Interaction of LaF_3 and ZrO_2. *Solid State Ionics* **1990**, *40−41*, 433−439.
(67) Choi, J. H.; Cui, P.; Lan, H.; Zhang, Z. Linear Scaling of the Exciton Binding Energy Versus the Band Gap of Two-Dimensional Materials. *Phys. Rev. Lett.* **2015**, *115*, 066403.
(68) Jiang, Z.; Liu, Z.; Li, Y.; Duan, W. Scaling Universality Between Band Gap and Exciton Binding Energy of Two-Dimensional Semiconductors. *Phys. Rev. Lett.* **2017**, *118*, 266401.
(69) Zasimov, P.; Amidani, L.; Retegan, M.; Walter, O.; Caciuffo, R.; Kvashnina, K. O. HERFD-XANES and RIXS Study on the Electronic Structure of Trivalent Lanthanides Across a Series of Isostructural Compounds. *Inorg. Chem.* **2022**, *61*, 1817−1830.
(70) Tanner, P. A.; Yeung, Y. Y. Nephelauxetic Effects in the Electronic Spectra of Pr^{3+}. *J. Phys. Chem. A* **2013**, *117*, 10726.
(71) Carnall, W. T.; Fields, P. R.; Rajnak, K. Electronic Energy Levels in the Trivalent Lanthanide Aquo Ions. I. Pr^{3+}, Nd^{3+}, Pm^{3+}, Sm^{3+}, Dy^{3+}, Ho^{3+}, Er^{3+}, and Tm^{3+}. *J. Chem. Phys.* **1968**, *49*, 4424−4442.
(72) Koshmak, K.; Banshchikov, A.; Vergentev, T.; Montecchi, M.; Céolin, D.; Rueff, J. P.; Sokolov, N. S.; Pasquali, L. High-Energy X-Ray Photoemission and Structural Study of Ultrapure LaF_3 Superionic Conductor Thin Films on Si. *J. Phys. Chem. C* **2014**, *118*, 10122−10130.
(73) Schneider, W. D.; Delley, B.; Wuilloud, E.; Imer, J. M.; Baer, Y. Electron-Spectroscopic Manifestations of the 4f States in Light Rare-Earth Solids. *Phys. Rev. B* **1985**, *32*, 6819−6831.
(74) Wu, S.; Cheng, L.; Wang, Q. Excitonic Effects and Related Properties in Semiconductor Nanostructures: Roles of Size and Dimensionality. *Mater. Res. Express* **2017**, *4*, 085017.
(75) Baskoutas, S.; Terzis, A. F. Size-Dependent Band Gap of Colloidal Quantum Dots. *J. Appl. Phys.* **2006**, *99*, 013708.

https://doi.org/10.1021/acs.jpcc.3c02011
J. Phys. Chem. C 2023, 127, 11111−11118